Single Self-Assembled InAs/GaAs Quantum Dots in Photonic Nanostructures: The Role of Nanofabrication

Jin Liu,[1,2,3,*] Kumarasiri Konthasinghe,[4] Marcelo Davanço,[1] John Lawall,[5] Vikas Anant,[6] Varun Verma,[7] Richard Mirin,[7] Sae Woo Nam,[7] Jin Dong Song,[8] Ben Ma,[9,10,11] Ze Sheng Chen,[9,10,11] Hai Qiao Ni,[9,10,11] Zhi Chuan Niu,[9,10,11] and Kartik Srinivasan[1,†]

[1]*Center for Nanoscale Science and Technology, National Institute of Standards and Technology, Gaithersburg, Maryland 20899, USA*
[2]*School of Physics, Sun-Yat Sen University, Guangzhou 510275, China*
[3]*Maryland NanoCenter, University of Maryland, College Park, Maryland 20742, USA*
[4]*Department of Physics, University of South Florida, Tampa, Florida 33620, USA*
[5]*Physical Measurement Laboratory, National Institute of Standards and Technology, Gaithersburg, Maryland 20899, USA*
[6]*Photon Spot, Inc., Monrovia, California 91016, USA*
[7]*National Institute of Standards and Technology, Boulder, Colorado 80305, USA*
[8]*Center for Opto-Electronic Materials and Devices Research, Korea Institute of Science and Technology, Seoul 136-791, South Korea*
[9]*State Key Laboratory for Superlattice and Microstructures, Institute of Semiconductors, Chinese Academy of Sciences, Beijing 100083, China*
[10]*College of Materials Science and Opto-Electronic Technology, University of Chinese Academy of Sciences, Beijing 100049, China*
[11]*Synergetic Innovation Center of Quantum Information and Quantum Physics, University of Science and Technology of China, Hefei, Anhui 230026, China*

(Received 13 December 2017; revised manuscript received 26 April 2018; published 13 June 2018)

Single self-assembled InAs/GaAs quantum dots are a promising solid-state quantum technology, with which vacuum Rabi splitting, single-photon-level nonlinearities, and bright, pure, and indistinguishable single-photon generation have been demonstrated. For such achievements, nanofabrication is used to create structures in which the quantum dot preferentially interacts with strongly confined optical modes. An open question is the extent to which such nanofabrication may also have an adverse influence, through the creation of traps and surface states that could induce blinking, spectral diffusion, and dephasing. Here, we use photoluminescence imaging to locate the positions of single InAs/GaAs quantum dots with respect to alignment marks with <5 nm uncertainty, allowing us to measure their behavior before and after fabrication. We track the quantum-dot emission linewidth and photon statistics as a function of the distance from an etched surface and find that the linewidth is significantly broadened (up to several gigahertz) for etched surfaces within a couple hundred nanometers of the quantum dot. However, we do not observe an appreciable reduction of the quantum-dot radiative efficiency due to blinking. We also show that atomic-layer deposition can stabilize spectral diffusion of the quantum-dot emission and partially recover its linewidth.

DOI: 10.1103/PhysRevApplied.9.064019

I. INTRODUCTION

Resonance fluorescence experiments have established that single InAs/GaAs self-assembled quantum dots (QDs) can exhibit Fourier-transform-limited emission, and as a result the individual photons emitted by these QDs can be nearly perfectly indistinguishable [1–3]. Because the collection of emission from an InAs/GaAs QD in bulk, as-grown material is limited to $<1\%$ due to the total internal reflection that results from the large refractive-index contrast between GaAs and air, the efficient extraction of the emitted light typically requires a modification of the photonic environment surrounding the QD. Such modifications should ideally not adversely influence the photon indistinguishability, and, recently, micropillar cavities have been able to achieve both high brightness and near-unity indistinguishability [4–7]. In comparison, more tightly confined geometries, such as photonic nanowires, photonic-crystal cavities, and suspended waveguides, generally have not exhibited such a

*liujin23@mail.sysu.edu.cn
†kartik.srinivasan@nist.gov

high degree of indistinguishability [8–13]. While this can partly be attributed to challenges in achieving high-quality resonance fluorescence in such structures (e.g., adequate suppression of the excitation laser and full control of the QD charge environment), another possibility is that the nanofabrication processes by which such structures are created may be an issue, mostly due to the plasma dry-etching processes involved. In particular, the fabrication of structures such as photonic crystals results in the presence of etched surfaces that are within a few hundred nanometers of the QD, and the potential influence of such surfaces on the QD emission, through coupling to surface states and charge traps, for example, is of significant concern. However, such a nanofabrication-induced effect has not been directly observed so far, in part due to the low photon-extraction efficiency of QDs in bulk, inefficient single-photon detection in the 900-nm band, and challenges in tracking single QDs before and after the nanofabrication process.

To unequivocally investigate this effect, QD epitaxy with distributed Bragg reflectors and superconducting nanowire single-photon detectors (SNSPDs) optimized in the 900-nm band (quantum efficiency $> 80\%$) are used to enable the efficient characterization of single QDs in bulk before any nanostructure fabrication. We utilize a recently developed nanoscale optical positioning technique [14,15] to locate the position of those QDs with respect to alignment features with an uncertainty of <5 nm. Subsequent aligned electron-beam lithography and dry etching allows us to place the QDs at specified positions away from etched surfaces. By measuring the QD emission linewidth and photon statistics before and after the fabrication steps for a number of samples, we are able to directly assess the influence that nanofabrication has on these important quantities, which in part characterizes the quality of single-photon emission that is possible from these systems. We determine that etched surfaces that are within 300 nm of the QDs broaden their emission under wetting layer excitation, while blinking, though observable in systems for which the etched surfaces are 100 nm away, generally does not appreciably influence the QD radiative efficiency. Finally, we find that the QDs that are closest to etched features have some emission lines that exhibit strong spectral diffusion, with timescales of a few seconds and a spectral wandering range of several nanometers. Such emission lines are greatly stabilized through atomic-layer deposition of an Al_2O_3 cap, which also produces a partial reduction in the homogeneous linewidth of the more stable (lower spectral diffusion) states. In agreement with recent progress in generating indistinguishable single photons via charge stabilization techniques in *p-i-n* structures [6,13], our results suggest that control of the charge environment is likely to be necessary to achieve Fourier-transform-limited emission in nanoscale device geometries.

II. SAMPLE FABRICATION AND MEASUREMENT SETUP

We consider two circularly symmetric geometries to assess the influence of nanoscale etched features on QD behavior. The first is the suspended circular Bragg grating geometry previously studied in Refs. [14,16]. This geometry, which consists of a central circular region (diameter of 1.2 μm) surrounded by etched circular grooves, can improve the radiative properties of the QD, through coupling to a localized cavity mode that enables Purcell enhancement of the QD radiative rate and preferential upwards emission with a relatively narrow divergence angle. The potential adverse effects of this geometry, in terms of an increased QD emission linewidth (e.g., due to spectral diffusion or additional dephasing channels) or the introduction of additional dark states, has not yet been systematically investigated. While a previous study [17] indicated that multiple timescale blinking of QDs in these cavities could result in a significant decrease in the radiative efficiency below unity, the QDs were not studied prior to device fabrication so that it was not possible to assess the role that etched surfaces played in the creation of the dark states that induced blinking.

The second structure is a nanopillar with a circular cross section. This is chosen as a convenient means to place etched surfaces within the vicinity of a QD, and we vary the pillar diameter across devices from 100 to 600 nm so that the maximum distance the QD can be from an etched surface is between 50 and 300 nm. The QD epitaxy [18] contains a layer of InAs QDs embedded within a 160-nm-thick GaAs layer (80 nm below the surface) and makes use of an underlying distributed Bragg reflector (DBR) consisting of 24 pairs of $Al_{0.9}Ga_{0.1}As$ /GaAs $\lambda/4$ layers to enhance the upwards vertical emission for the QDs in bulk and nanopillar geometries. It also contains a 1000-nm-thick $Al_{0.7}Ga_{0.3}As$ sacrificial layer, placed in between the QD-containing layer and the DBR, which allows the aforementioned suspended grating microcavities to be fabricated from the same epitaxy so that the growth conditions are fixed across all samples.

After fabricating metallic alignment marks on the sample, we use our recently developed photoluminescence imaging system [7,15], shown schematically in Fig. 1, to locate the positions of single QDs with a one-standard-deviation uncertainty of < 5 nm. This technique relies on wide-field excitation of QDs within an approximately 66 μm $\times$ 66 μm field of view using a short-wavelength LED and the simultaneous illumination of the sample surface (including metallic alignment marks) using a second, longer-wavelength LED. Emission from the QDs and reflected illumination light are separated from unwanted light using filters and sent to a sensitive camera, where the generated image is analyzed using a maximum-likelihood estimator and a cross-correlation approach for identifying the centers of the QD emission and alignment marks, respectively. The QD locations are

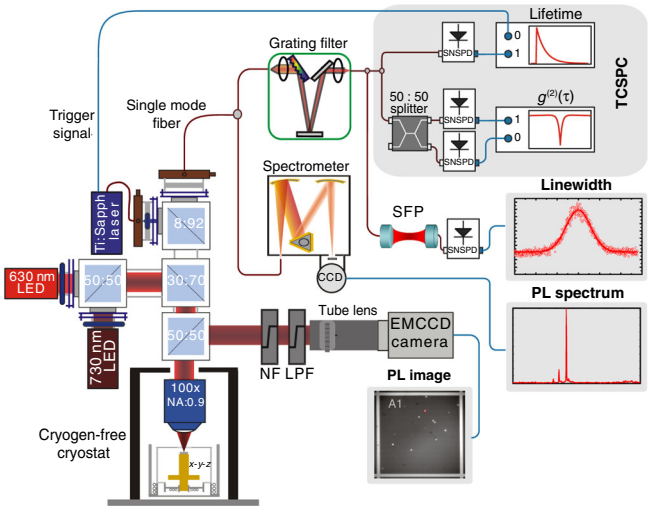

FIG. 1. *Experimental setup.* Photoluminescence (PL) images are generated by exciting the sample simultaneously with 630- and 730-nm LEDs, with PL from the QDs and reflected 730-nm light from the alignment marks separated from unwanted light through 800-nm band notch filters (NFs) and a 700-nm long-pass filter (LPF), and sent into an electron-multiplying charge-coupled device (EMCCD) camera. PL spectra from specific QDs within the image are obtained by pumping them with a fiber-coupled Ti:sapphire laser whose wavelength is tuned to the wetting layer (spot diameter $< 5\ \mu$m), collecting the emission into a single-mode fiber, and sending it into a grating spectrometer. Time-correlated single-photon-counting (TCSPC) measurements are performed by sending the collected emission into a fiber-coupled tunable grating filter, with the filtered signal then going into either one SNSPD for lifetime measurements or into a 50:50 fiber coupler and two SNSPDs for intensity autocorrelation measurements. Alternately, the filtered signal can be sent into a scanning Fabry-Perot (SFP) cavity for high-resolution spectroscopy, where the output of the SFP is again coupled into a SNSPD.

used in subsequent device fabrication, which consists of aligned electron-beam lithography, plasma etching of the QD-containing GaAs layer, resist removal, and, in the case of the circular grating cavities, a hydrofluoric acid etch to remove the $Al_{0.7}Ga_{0.3}As$ sacrificial layer.

Our photoluminescence imaging system also contains a confocal path for the excitation of individual QDs using a continuous-wave Ti:sapphire laser and collection of QD emission into a single-mode fiber. The QDs are all excited at the wetting layer transition wavelength (approximately 850 nm), as successful excitation through lower-energy states (e.g., quasiresonant excitation via the QD p shell or resonant excitation of the QD transition) is not consistently observed for all QDs. Collected emission is sent either into a grating spectrometer for spectral analysis or through a tunable grating filter for spectral isolation of individual QD transitions. Isolated QD lines are then sent into a scanning Fabry-Perot (SFP) cavity for high-resolution (200-MHz) linewidth analysis or through a 50:50 fiber-coupled beam splitter and into two SNSPDs and a time-correlated single-photon-counting (TCSPC) card for measurement of the intensity autocorrelation function $[g^{(2)}(\tau)]$. Finally, a pulsed excitation source is used for measurements of the radiative decay of a given QD transition. All measurements are performed on the same QD both before and after device fabrication.

III. CIRCULAR BRAGG GRATING DEVICES

Figure 2 shows representative results for the circular Bragg grating cavities. QDs within field $A1$ are located using the aforementioned imaging approach [Fig. 2(a)], and circular Bragg grating cavities are fabricated around two of the located QDs [Fig. 2(b)]. The effects of the microcavity on the QD radiative properties are clearly seen in Figs. 2(c) and 2(d) and consist of a strong increase in the collected emission under saturated excitation [Fig. 2(c)] and an approximately 2.5× reduction in the QD radiative lifetime of the 911-nm transition line [Fig. 2(d)]. Considering the approximately 3.6-nm detuning between the QD and cavity mode line center, this level of Purcell enhancement is consistent with the QD being spatially offset from the center of the device by no more than 50 nm [14]. Encouragingly, we also do not observe any adverse influence of fabrication, as evidenced by measurements of the linewidth [Fig. 2(e)] and the intensity autocorrelation function $[g^{(2)}(\tau)]$ of this QD transition [Figs. 2(f)–2(h)].

In the $g^{(2)}(\tau)$ measurement, we have recorded data over a duration long enough to enable its evaluation over 10 orders of magnitude in time [Fig. 2(f)]. As discussed in Ref. [17] in the context of InAs/GaAs QDs and in several earlier works focused on the behavior of single molecules and colloidal QDs [19], the measurement of $g^{(2)}(\tau)$ out to sufficiently long timescales can be a preferred approach for studying blinking in single quantum emitters. In particular, while a time record of the fluorescence intensity is sensitive to the time-bin width chosen (photon shot noise dominates for too-small bins; shorter timescale behavior is washed out for too-long bins) and subsequent histogramming analysis is influenced by the choice of a threshold intensity level, $g^{(2)}(\tau)$ does not require the selection of such potentially arbitrary input parameters [20]. Blinking is evidenced in the $g^{(2)}(\tau)$ data by bunching ($g^{(2)} > 1$) after the initial antibunching dip at $\tau = 0$, and the subsequent transition to the Poissonian level $[g^{(2)}(\tau) = 1]$ can occur over second-long timescales and is potentially punctuated by several steps. In Ref. [17], such behavior is well reproduced by a model in which the radiative transition is coupled to multiple dark states, with each dark state responsible for a step in $g^{(2)}(\tau)$ and showing a characteristic occupancy and population and depopulation rate. The physical mechanisms for blinking in epitaxial QDs are multitude: carrier traps formed by the defects in the vicinity of QDs [21], perturbation of the

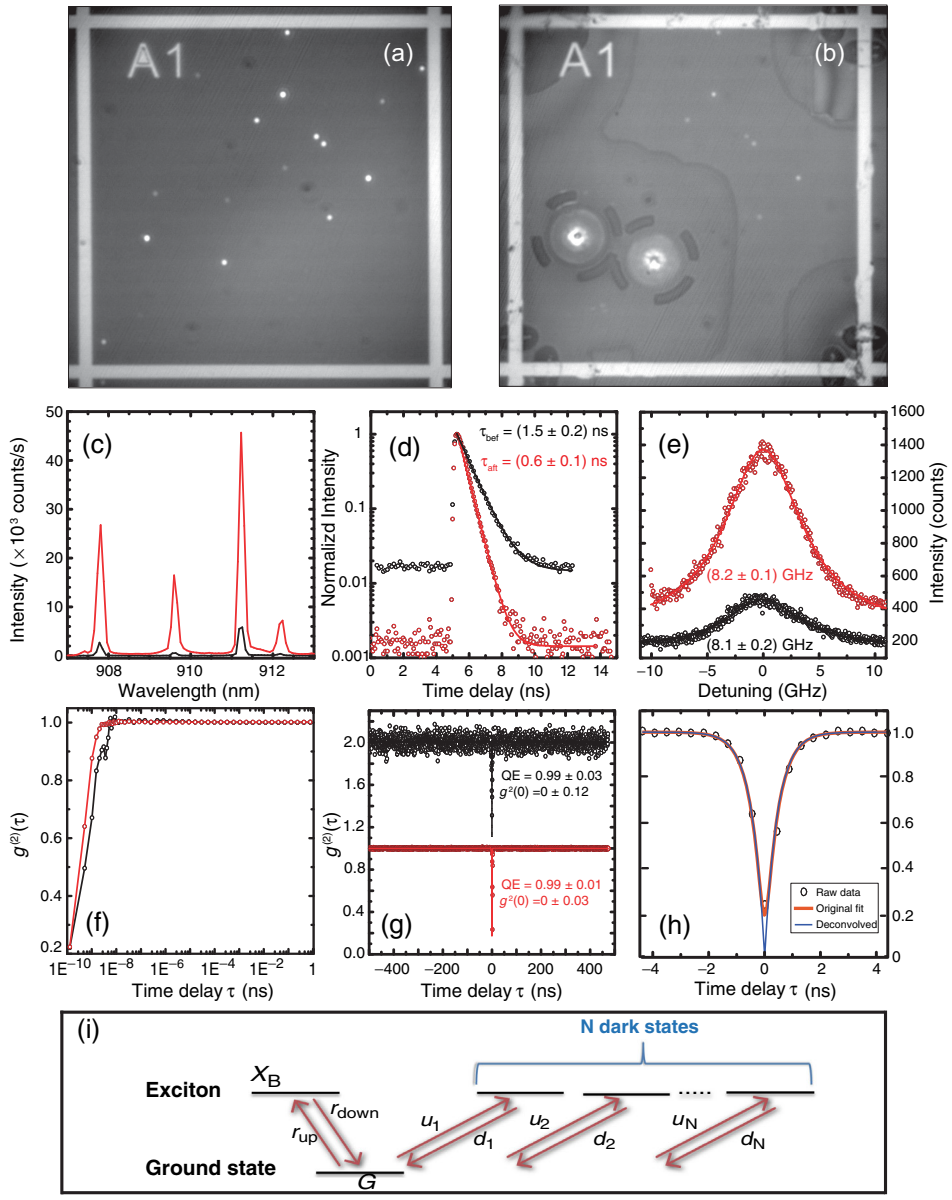

FIG. 2. *QDs in circular Bragg grating cavities.* The optical properties of QDs before and after the creation of circular Bragg gratings are measured. (a),(b) Photoluminescence images of the QDs (a) before and (b) after device fabrication. The alignment mark separation is 50 μm. (c) Photoluminescence spectrum, (d) photoluminescence decay, (e) emission linewidth, and (f)–(h) intensity autocorrelation recorded for one of the QDs before (black lines and circles) and after (red lines and circles) fabrication, under wetting layer excitation. The data in (d)–(h) are taken for the brightest emission line in the spectrum from (c) (near 911 nm). The photoluminescence decay data in (d) are fit to a monoexponentially decaying function, and a lifetime $\tau_{\mathrm{bef}} = 1.5 \pm 0.2$ ns ($\tau_{\mathrm{after}} = 0.6 \pm 0.1$ ns) is extracted for the QD state before (after) fabrication, where the uncertainty is a one-standard-deviation value from the fit. The emission linewidth data (circles) in (e), measured by the SFP cavity, are fit to a Gaussian function (solid line) to determine the full width at half maximum listed on the plot, with the uncertainty being a one-standard-deviation value from the fit. The intensity autocorrelation measurement in (f) is recorded over a duration long enough to enable the evaluation of $g^{(2)}(\tau)$ out to a time delay as long as 1 s, and the time axis is given in a logarithmic scale. The intensity autocorrelation measurements in (g) and (h) are presented over a narrower range of time delays, to focus on the antibunching dip and potential presence of shorter timescale blinking. For both the before- and after-fabrication data in (g), the quantum efficiency (QE) is extracted from a three-level system fit to the data, as described in the main text, and the uncertainty value is a one-standard-deviation value from the fit. The quoted $g^{(2)}(0)$ values are determined by additionally deconvolving the SNSPD or TCSPC timing response from the fit. An enlarged view of the raw data, fit (no deconvolution), and fit including deconvolution is shown in (h), for the QD state after device fabrication. The before-fabrication data in (g) are vertically shifted up by 1.0 units for clarity. (i) Energy level diagram of the model used in blinking studies. X_B, X_D, and G, are the optically bright, dark, and ground states of the exciton, respectively. The QD is pumped from the ground state G with a rate of r_{up}, the bright state X_B decays to the ground state with a spontaneous decay rate r_{down}.

electron and hole wave-function overlap by the local electrical fields of trapped charges [22], and spectral shifts induced by the tunneling of carriers into nearby traps [23].

A Hanbury-Brown and Twiss setup is used to obtain the second-order correlation function $g^{(2)}(\tau)$ of the QD emission upon continuous-wave pumping at the saturation power. We record single-photon detection events with a time correlator in the time-tagged mode for 2 or 4 hr, depending on the count rates in the SNSPDs. We fit the $g^{(2)}(\tau)$ data, including the convolution of the detector response, by using a rate-equation model in which a bright exciton transition is coupled to multiple dark states, as shown in Fig. 2(i). The population p of each state evolves according to the rate equations

$$\frac{dp_{X_B}}{d\tau} = r_{\text{up}} p_G - r_{\text{down}} p_{X_B},$$
$$\frac{dp_G}{d\tau} = r_{\text{down}} p_{X_B} + \sum_i d_i p_i - \sum_i u_i p_{X_G},$$
$$\frac{dp_i}{d\tau} = u_i p_{X_G} - d_i p_i.$$

In such a model, each dark state is populated at a rate u_i and depopulated at a rate d_i, and all parameters are varied in the fit except for the radiative decay rate r_{down}, which is determined from independent lifetime measurements. The optical transitions measured in this work are all single-exciton states, revealed by the power-dependent fluorescence measurements, and the $g^{(2)}(\tau)$ data can be very well fitted with only one dark state. The quantum efficiencies of the QDs then are extracted from the estimation of the dark-state occupancy.

Here, we see no pronounced bunching or multiple dark-state behavior, in either the before- or after-fabrication data in Fig. 2(f). Because $g^{(2)}(\tau) = 1$ for $\tau > 10$ ns (in contrast, in Ref. [17], the Poissonian level was reached only at microsecond or even 100-ms timescales), we zoom in on the region within ± 500 ns of $\tau = 0$ in Fig. 2(g) and analyze the data by fitting it to the three-level model in which the radiative transition is coupled to a single dark state (see Supplemental Material [18]).

The SFP-measured homogeneous linewidth is essentially unchanged at approximately 8 GHz, while the enhancement of the single-photon-extraction efficiency is clearly seen from the photon counts in the SFP measurement. In the circular Bragg grating geometries, both radiative decay rates and single-photon collection efficiency of single QDs are significantly enhanced by coupling to the confined cavity mode, while other crucial properties (i.e., linewidth and quantum efficiency) are unchanged, which is highly desirable for realizing bright and coherent single-photon sources for quantum-information processing tasks.

IV. NANOPILLAR DEVICES

The linewidth-broadening effect induced by smooth epitaxial interfaces parallel to the sample surface has previously been studied in detail with superlattice structures [24,25]. In our study, the combination of high-accuracy QD positioning and high-resolution linewidth measurements allows us to investigate influences from the etched sidewalls that are ubiquitous in planar nanophotonic devices. Such dry-etched surfaces usually experience a combination of strong physical ion bombardment and complicated chemical-reaction processes and are potentially more likely to introduce surface traps or states than the very smooth epitaxial interfaces studied in Refs. [24,25].

In a circular Bragg grating cavity containing a single, accurately positioned QD, the nearest etched surface is approximately 600 nm away from the QD. Such a relatively large separation ensures that the confined exciton states in the QD are immune to the influence of any surface traps or states created by the dry-etching process. On the other hand, more tightly confined optical modes with a sub-cubic-wavelength scale volume are highly desirable for achieving a stronger light-matter interaction, e.g., the strong coupling regime with its accompanying single-photon-level nonlinearity. In such small-mode-volume nanophotonic structures, such as photonic-crystal cavities, it is often inevitable that the optimal position for QD-field interaction will be within the vicinity (few hundred nanometers) of etched surfaces. Thus, we fabricate QD-containing nanopillars with different diameters, to further investigate the influences of etched surfaces on QDs that are nominally 50, 100, and 300 nm away from the dry-etched sidewalls, shown in Figs. 3(a)–3(c). Since there is neither an engineered cavity resonance nor far-field reshaping effect, we do not expect any pronounced Purcell effect and collection efficiency enhancement in these nanopillars. Again, we focus on the optical properties (i.e., blinking and linewidth) that are crucial for single-photon generation and potentially influenced by the presence of the etched surfaces.

For the QD that is nominally 50 nm away from the etched surface [Fig. 3(a)], a very small bunching peak near zero time delay is observed in the $g^{(2)}(\tau)$ measurement, which is a signature of coupling to the dark states [Fig. 3(d)]. By fitting the long-time scale $g^{(2)}(\tau)$ with the three-level-system model (see Supplemental Material [18]), we extract a quantum efficiency of 0.99 ± 0.01, which is nearly unchanged compared to the value before fabrication, indicating that the coupling to any dark states that is induced by the etched surfaces is too small to appreciably change the quantum efficiency of the QD. This is strikingly different from the case in Ref. [17], in which coupling to dark states lowers the quantum efficiency of the QD down to 78% (see the comparison of

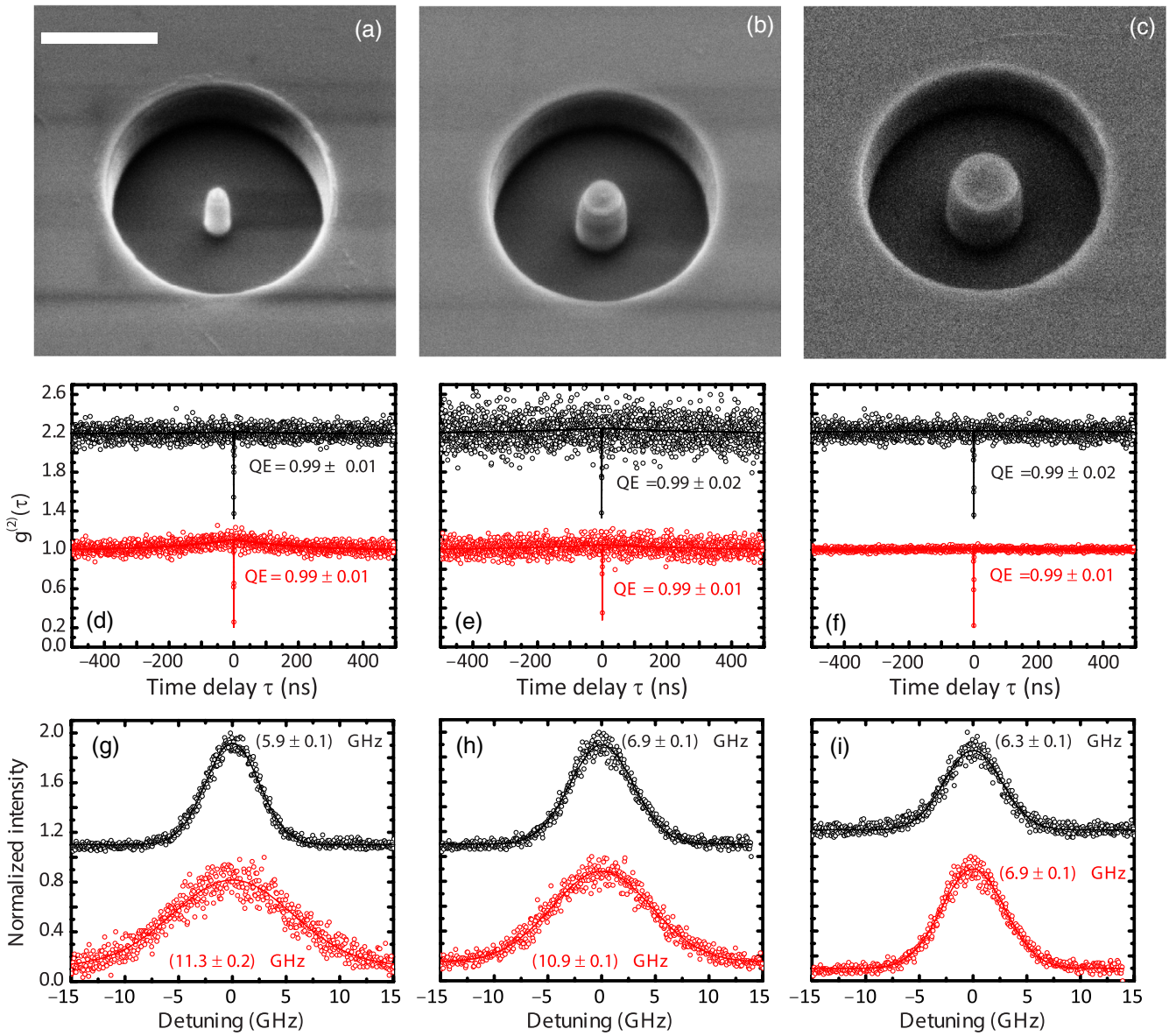

FIG. 3. *Behavior of QDs in etched nanopillars.* Behavior of QDs before (black lines and circles) and after (red lines and circles) fabrication of nanopillars of varying diameter, under wetting layer excitation. (a) Scanning electron microscope (SEM) image, (d) intensity autocorrelation, and (g) emission linewidth for a QD in the smallest nanopillar fabricated, with a nominal diameter of 100 nm. (b) SEM image, (e) intensity autocorrelation, and (h) emission linewidth for a QD in a nanopillar with a nominal diameter of 300 nm. (c) SEM image, (g) intensity autocorrelation, and (i) emission linewidth for a QD in a nanopillar with a nominal diameter of 600 nm. The before-fabrication data in (d)–(f) are vertically shifted up by 1.2 units for clarity. The QE values in (d)–(f) are extracted from a three-level system fit to the data (solid lines), as described in the main text, and the uncertainty value is a one-standard-deviation value from the fit. The emission linewidth data in (g)–(i) are fit to Gaussians to determine the full width at half maximum listed on the plots, with the uncertainties being one-standard-deviation values from the fits. The scale bar displayed in (a) represents 1000 nm and is applicable to the SEM images in (b) and (c) as well.

QE between Ref. [17] and this work in Supplemental Material [18]). We note that in our previous work, in which the QD was not characterized prefabrication [17], it was not possible to determine whether blinking is an intrinsic property of the as-grown QD, e.g., potentially due to the introduction of defects during growth, or whether it is induced by either pre-etch sample annealing [26] or the etch process. The present data strongly indicate that etching likely did not play a big role.

The linewidth of the QD that is 50 nm away from the etched surface is more sensitive than the quantum efficiency and broadened by a factor of approximately 1.9 [Fig. 3(g)]. We postulate that such a linewidth broadening is mainly due to the spectral diffusion

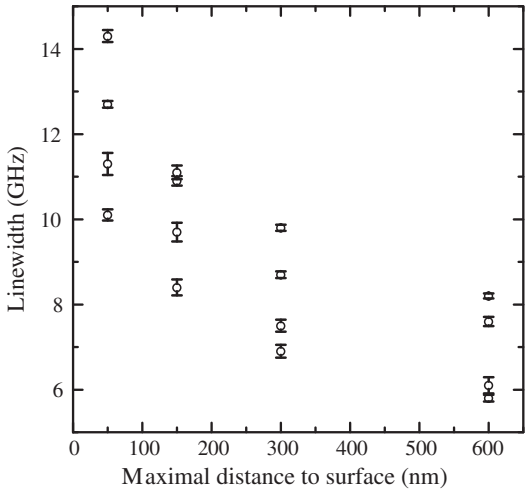

FIG. 4. *Linewidth of QDs as a function of the proximity to etched surfaces.* Compilation of QD emission linewidths under wetting layer excitation as a function of the maximum distance between the QD and an etched surface. For the circularly symmetric structures studied in this work, this is given by the radius of the central region of the circular Bragg grating (Fig. 2) and the radius of the nanopillar 80 nm below the top surface (Fig. 3). The emission linewidth is measured by the SFP method, and the error bars are given by the one-standard-deviation uncertainties from nonlinear least-squares fits of the data to Gaussian functions.

induced by the charge states on the etched surfaces. By moving the QD to nominally 150 nm away from the surface [Fig. 3(b)], the bunching near the zero delay in the $g^{(2)}(\tau)$ curve is almost negligible, resulting in an unchanged quantum efficiency after the fabrication. The linewidth-broadening factor is reduced to 1.72, indicating an alleviated influence from the etched surface. Once the QD is nominally 300 nm away from the etched surface [Fig. 3(c)], we barely observe any changes either in $g^{(2)}(\tau)$ or in the linewidth measurement [Figs. 3(f) and 3(i), respectively].

Although it is very informative to measure the linewidth of the same QDs before and after the fabrication, the very long characterization time of these measurements prevents us from obtaining a large sample of data for additional statistical analysis. Thus, we position a number of QDs in nanopillars with various sizes without systematic optical characterization prior to the fabrication. Figure 4 presents the statistics of the linewidth of QDs with different maximal distances to the etched surfaces. We clearly see that the linewidth-broadening effect is significantly reduced by moving the QDs away from the etched surface. The critical distance to avoid the surface charges is approximately 300 nm, for which the linewidth of QDs is close to the number for bulk QDs. We note that the average linewidth of the QDs in bulk is approximately 6 GHz under the wetting layer excitation scheme used in this work. A more sensitive probe of the charge environment could be achieved by using a resonant excitation scheme [25]; however, the QDs used in this study do not exhibit resonance fluorescence signals. In particular, resonance fluorescence is not observed, even if a weak, nonresonant ancillary laser is applied to stabilize the charge environment [27]. We note that, despite several impressive demonstrations of resonance fluorescence in different QD systems, its observation is not yet universal and can vary significantly from wafer to wafer.

V. SURFACE PASSIVATION VIA ATOMIC-LAYER DEPOSITION

Because of the uncertainties from the *e*-beam lithography and the optical positioning process, we could occasionally achieve a situation where the QDs are less than 50 nm away from the etched surfaces. These QDs typically exhibit severe spectral wandering on a timescale of a few seconds [28], as shown in Fig. 5(a). The single QD shows two typical spectral characteristics: several emission lines with slightly varying wavelength and a single emission line that jumps across a range of a few nanometers. Since surface treatments have been demonstrated as very effective ways to improve emission and reduce absorption in III-V material [29,30], we employ an atomic-layer-deposition (ALD) process to deposit a thin capping layer of Al_2O_3 for stabilizing the charge environment on the etched surfaces. After depositing a 15-nm Al_2O_3 capping layer, the large spectral wandering effect is completely suppressed, and the single QD emission line is stabilized with an enhanced emission intensity, as shown in Fig. 5(b). The suppression of spectral wandering can be further appreciated in Figs. 5(c) and 5(d) showing the histogram of the QD's center emission wavelength in Figs. 5(a) and 5(b) respectively. Prior to the ALD process, the higher counts near to 916 and 920 nm correspond to the multiexciton complex states with several emission lines, while the low counts in between reveal the wavelength shifting of the single exciton state, shown in Fig. 5(c). The stable single-emission line due to the effective removal of the surface charges by ALD results in a δ-function-like histogram in Fig. 5(d).

We further apply the ALD process to the nanopillar devices from the previous section (which do not exhibit large spectral wandering) and investigate the surface passivation effect on the QD linewidth. Figures 5(e)–5(g) present the linewidth of the QDs shown in Figs. 3(g)–3(i), with and without the ALD process. The linewidth of the QDs in the nanopillar devices is indeed reduced; however, it does not fully recover to the value prior to dry etching. Further linewidth reduction is not observed with an extra deposition of 15-nm Al_2O_3, indicating that the charge stabilization induced by Al_2O_3 has been fully established with only one ALD step. The stabilization of the QD emission lines and partially recovered linewidth by the ALD process suggest that surface passivation processes could be a viable method to remedy the adverse effects introduced by the presence of etched surfaces that results from the fabrication of nanophotonic devices.

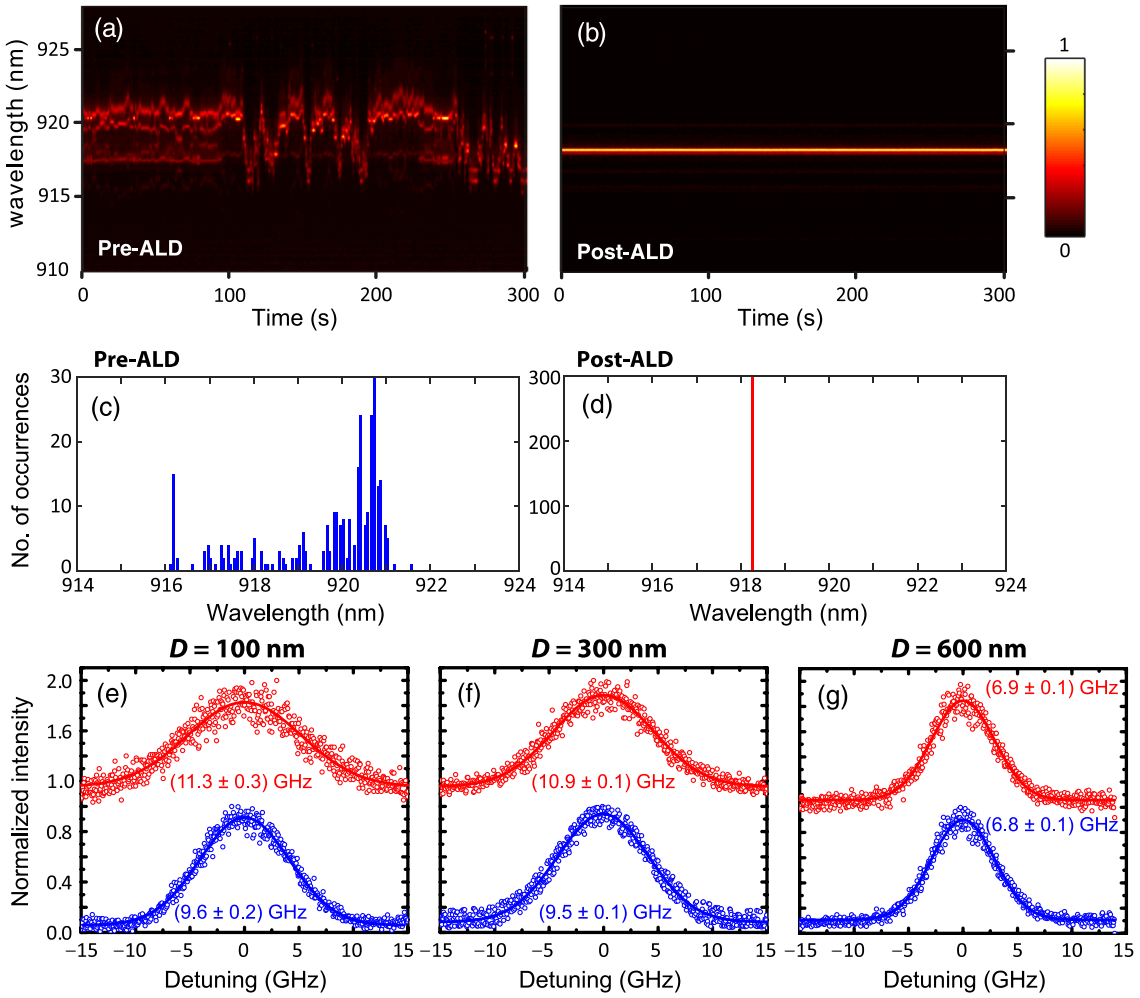

FIG. 5. *Stabilizing QD emission through atomic-layer deposition.* Photoluminescence spectrum, recorded as a function of the time in 1-s acquisition intervals, for a QD (a) before and (b) after ALD of an Al_2O_3 capping layer. In each case, the emission intensity is normalized to the maximum value within the spectrum (scale bar shown to the right). (c) and (d) are the histograms of the photon counts as a function of the wavelength in (a) and (b), respectively, with a spectral bin size of 0.05 nm. (e)–(g) Emission linewidth for QDs in nanopillars before (red lines and circles) and after (blue lines and circles) ALD. The nanopillar diameters are (e) 100 nm, (f) 300 nm, and (g) 600 nm. The emission linewidth is measured by the SFP method, and the uncertainties are given by the one-standard-deviation uncertainties from nonlinear least-squares fits of the data to Gaussian functions.

VI. DISCUSSION

In conclusion, we directly and quantitatively investigate the influence of nanofabrication on the optical properties of single QDs via a fluorescence-imaging-based QD positioning technique, thereby shedding light on considerations that must be taken into account when designing and building high-performance QD-based quantum photonic devices via modern nanofabrication processes. First, by positioning QDs in the center of circular Bragg grating cavities, approximately 600 nm away from etched surfaces, we find that we can simultaneously increase both the decay rate and the collection efficiency of the QD, without compromising its optical properties. We then consider nanopillar geometries in which the separation of the QD from the etched surfaces is reduced. While the quantum efficiency of single QDs is rather insensitive to the surfaces, the linewidth starts to broaden once the QD is within 300 nm of the surface, at which point charged surface states appear to play an important role. Strong spectral wandering is observed when the distances between the QDs and surfaces are less than 50 nm. An ALD process is successfully applied to completely suppress the strong spectral wandering and partially reduce the linewidth broadening.

Despite the broadening effect for QDs with lifetime-limited linewidth not being directly observed via resonance fluorescence signals in our study, the significant influence of the etched surface on QDs with a broadened linewidth strongly indicates that the narrow-linewidth QDs (under resonant excitation) are very likely to be broadened by the same QD-surface separation or larger, and this further points to the need to control the charging

environment, either through electrodes [3,6,13], potentially a nonresonant laser [27], or ALD or surface passivation, as we show. In the future, higher-resolution spectroscopy, e.g., based on resonance fluorescence, is highly desirable to fully probe the adverse effects from the nanofabrication process. Such measurements could better elucidate the role of spectral wandering on the observed linewidth broadening [25]. Controlling such spectral wandering will likely require some form of charge stabilization, as has recently been successfully applied by a number of groups through the use of *p-i-n* structures to enable high-performance single-photon sources [3,6,13]. Further implementation of such *p-i-n* structures in nanophotonic devices with ultrasmall mode volumes may impose formidable technical challenges on the fabrication process. Alternatively, surface passivation could serve as a potentially important approach to stabilize the charge environment without introducing designs that require electrical contacts. Thus, more advanced surface passivation techniques than the ALD approach presented here could be pursued to maximally limit the influences of charged states from the etched surfaces.

ACKNOWLEDGMENTS

J. L. acknowledges support under the Ministry of Science and Technology of China (Grants No. 2018YFA0306100 and No. 2016YFA0301300), the National Natural Science Foundation of China (Grant No. 11304102), Guangzhou Science and Technology project (Grant No. 201805010004), and the Cooperative Research Agreement between the University of Maryland and NIST-CNST, Grant No. 70NANB10H193. Z. C. N. acknowledges support under the National Natural Science Foundation of China (91321313).

[1] C. Matthiesen, M. Geller, C. H. H. Schulte, C. L. Gall, J. Hanson, Z. Y. Li, M. Hugues, E. Clarke, and M. Atature, Phase-locked indistinguishable photons with synthesized waveforms from a solid-state source, Nat. Commun. **4**, 1600 (2013).

[2] Y.-M. He, Y. He, Y.-J. Wei, D. Wu, M. Atature, C. Schneider, S. Höfling, M. Kamp, C.-Y. Lu, and J.-W. Pan, On-demand semiconductor single-photon source with near-unity indistinguishability, Nat. Nanotechnol. **8**, 213 (2013).

[3] A. V. Kuhlmann, J. H. Prechtel, J. Houel, A. Ludwig, D. Reuter, A. D. Wieck, and R. J. Warburton, Transform-limited single photons from a single quantum dot, Nat. Commun. **6**, 8204 (2015).

[4] S. Unsleber, Y.-M. He, S. Gerhardt, S. Maier, C.-Y. Lu, J.-W. Pan, N. Gregersen, M. Kamp, C. Schneider, and S. Höfling, Highly indistinguishable on-demand resonance fluorescence photons from a deterministic quantum dot micropillar device with 74% extraction efficiency, Opt. Express **24**, 8539 (2016).

[5] X. Ding, Y. He, Z. C. Duan, N. Gregersen, M.-C. Chen, S. Unsleber, S. Maier, C. Schneider, M. Kamp, S. Höfling, C.-Y. Lu, and J.-W. Pan, On-Demand Single Photons with High Extraction Efficiency and Near-Unity Indistinguishability from a Resonantly Driven Quantum Dot in a Micropillar, Phys. Rev. Lett. **116**, 020401 (2016).

[6] N. Somaschi, V. Giesz, L. De Santis, J. C. Loredo, M. P. Almeida, G. Hornecker, S. L. Portalupi, T. Grange, C. Antn, J. Demory, C. Gmez, I. Sagnes, N. D. Lanzillotti-Kimura, A. Lematre, A. Auffeves, A. G. White, L. Lanco, and P. Senellart, Near-optimal single-photon sources in the solid state, Nat. Photonics **10**, 340 (2016).

[7] Y.-M. He, J. Liu, S. Maier, M. Emmerling, S. Gerhardt, M. Davanco, K. Srinivasan, C. Schneider, and S. Höfling, Deterministic implementation of a bright, on-demand single photon source with near-unity indistinguishability via quantum dot imaging, Optica **4**, 802 (2017).

[8] K. D. Jöns, P. Atkinson, M. Müller, M. Heldmaier, S. M. Ulrich, O. G. Schmidt, and P. Michler, Triggered indistinguishable single photons with narrow line widths from site-controlled quantum dots, Nano Lett. **13**, 126 (2013).

[9] S. Varoutsis, S. Laurent, P. Kramper, A. Lematre, I. Sagnes, I. Robert-Philip, and I. Abram, Restoration of photon indistinguishability in the emission of a semiconductor quantum dot, Phys. Rev. B **72**, 041303(R) (2005).

[10] K. H. Madsen, S. Ates, J. Liu, A. Javadi, S. M. Albrecht, I. Yeo, S. Stobbe, and P. Lodahl, Efficient out-coupling of high-purity single photons from a coherent quantum dot in a photonic-crystal cavity, Phys. Rev. B **90**, 155303 (2014).

[11] D. Englund, A. Faraon, B.-Y. Zhang, Y. Yamamoto, and J. Vuckovic, Generation and transfer of single photons on a photonic crystal chip, Opt. Express **15**, 5550 (2007).

[12] F. Liu, A. J. Brash, J. O'Hara, L. M. P. P. Martins, C. P. Phillips, R. J. Cole, B. Royall, E. Clarke, C. Bentham, N. Prtljaga, I. E. Itskevich, L. R. Wilson, M. S. Skolnick, and A. M. Fox, High Purcell factor generation of coherent on-chip single photons, arXiv:1706.04422.

[13] G. Kirsanske, H. Thyrrestrup, R. Daveau, C. L. Dreeen, T. Pregnolato, L. Midolo, P. Tighineanu, A. Javadi, S. Stobbe, R. Schott, A. Ludwig, A. D. Wieck, S. I. Park, J. D. Song, A. V. Kuhlmann, I. Söllner, M. C. Löbl, R. J. Warburton, and P. Lodahl, Indistinguishable and efficient single photons from a quantum dot in a planar nanobeam waveguide, Phys. Rev. B **96**, 165306 (2017).

[14] L. Sapienza, M. Davanco, A. Badolato, and K. Srinivasan, Nanoscale optical positioning of single quantum dots for bright and pure single-photon emission, Nat. Commun. **6**, 7833 (2015).

[15] J. Liu, M. Davanco, L. Sapienza, K. Konthasinghe, J. D. Song, A. Badolato, and K. Srinivasan, Cryogenic photoluminescence imaging system for nanoscale positioning of single quantum emitters, Rev. Sci. Instrum. **88**, 023116 (2017).

[16] M. Davanco, M. T. Rakher, D. Schun, A. Badolato, and K. Srinivasan, A circular dielectric grating for vertical extraction of single quantum dot emission, Appl. Phys. Lett. **99**, 041102 (2011).

[17] M. Davanco, C. S. Hellberg, S. Ates, A. Badolato, and K. Srinivasan, Multiple time scale blinking in InAs quantum dot single-photon sources, Phys. Rev. B **89**, 161303(R) (2014).

[18] See Supplemental Material at http://link.aps.org/supplemental/10.1103/PhysRevApplied.9.064019 for details on the epitaxial layer structure, fabrication process, and quantum efficiency calculations.

[19] B. Lounis and M. Orrit, Single-photon sources, Rep. Prog. Phys. **68**, 1129 (2005).

[20] Histogram analysis of the fluorescence intensity time record can be used to probe instantaneous intensity fluctuations and, in principle, be used to reveal probability distributions of emission on and off times, which can be associated with particular blinking mechanisms. However, in order for such an analysis to be reliable, the collected signal must obey a stringent set of of criteria [C. H. Crouch, O. Sauter, X. Wu, R. Purcell, C. Querner, M. Drndic, and M. Pelton, Nano Lett. **10**, 1692 (2010)], which may not be available depending on the experimental setup.

[21] X. Y. Wang, W. Q. Ma, J. Y. Zhang, G. J. Salamo, M. Xiao, and C. K. Shih, Photoluminescence intermittency of InGaAs/GaAs quantum dots confined in a planar microcavity, Nano Lett. **5**, 1873 (2005).

[22] M. Sugisaki, H. W. Ren, K. Nishi, and Y. Masumoto, Fluorescence Intermittency in Self-Assembled InP Quantum Dots, Phys. Rev. Lett. **86**, 4883 (2001).

[23] A. Berthelot, I. Favero, G. Cassabois, C. Voisin, C. Delalande, P. Roussignol, R. Ferreira, and J. M. Gerard, Unconventional motional narrowing in the optical spectrum of a semiconductor quantum dot, Nat. Phys. **2**, 759 (2006).

[24] C. F. Wang, A. Badolato, I. Wilson-Rae, P. M. Petroff, and E. Hu, Optical properties of single InAs quantum dots in close proximity to surfaces, Appl. Phys. Lett. **85**, 3423 (2004).

[25] J. Houel, A. V. Kuhlmann, L. Greuter, F. Xue, M. Poggio, B. D. Gerardot, P. A. Dalgarno, A. Badolato, P. M. Petroff, A. Ludwig, D. Reuter, A. D. Wieck, and R. J. Warburton, Probing Single-Charge Fluctuations at a GaAs/AlAs Interface Using Laser Spectroscopy on a Nearby InGaAs Quantum Dot, Phys. Rev. Lett. **108**, 119902(E) (2012).

[26] S. Malik, C. Roberts, and R. Murray, Tuning self-assembled InAs quantum dots by rapid thermal annealing, Appl. Phys. Lett. **71**, 1987 (1997).

[27] O. Gazzano, T. Huber, V. Loo, S. Polyakov, E. B. Flagg, and G. S. Solomon, Quantum dot resonant-fluorescence linewidth narrowing and enhanced intensity, arXiv:1702.03947.

[28] H. D. Robinson and B. B. Goldberg, Light-induced spectral diffusion in single self-assembled quantum dots, Phys. Rev. B **61**, R5086 (2000).

[29] I. Yeo, N. T. Malik, M. Munsch, E. Dupuy, J. Bleuse, Y.-M. Niquest, J.-M. Gerad, J. Claudon, E. Wagner, S. Seidelin, A. Auffeves, J.-P. Poizat, and G. Nogues, Surface effects in a semiconductor photonic nanowire and spectral stability of an embedded single quantum dot, Appl. Phys. Lett. **99**, 233106 (2011).

[30] B. Guha, F. Marsault, F. Cadiz, L. Morgenroth, V. Ulin, V. Berkovitz, A. Lematre, C. Gomez, A. Amo, S. Combrie, B. Gerard, G. Leo, and I. Favero, Surface-enhanced gallium arsenide photonic resonator with quality factor of 6×10^6, Optica **4**, 218 (2017).